AIMS Environmental Science, 4(1): 145-167.
DOI: 10.3934/environsci.2017.1.145
Received: 24 August 2016
Accepted: 03 February 2017
Published: 14 February 2017

http://www.aimspress.com/journal/environmental

Research article

Effects of rapid urbanisation on the urban thermal environment between 1990 and 2011 in Dhaka Megacity, Bangladesh

Lewis Trotter*, Ashraf Dewan and Todd Robinson

Department of Spatial Sciences, Curtin University, Kent Street Bentley, Building 207, Perth Western Australia 6845, Australia

*** Correspondence:** Email: lewis.trotter@postgrad.curtin.edu.au; Tel: +61-040-005-2137.

Abstract: This study investigates the influence of land-use/land-cover (LULC) change on land surface temperature (LST) in Dhaka Megacity, Bangladesh during a period of rapid urbanisation. LST was derived from Landsat 5 TM scenes captured in 1990, 2000 and 2011 and compared to contemporaneous LULC maps. We compared index-based and linear spectral mixture analysis (LSMA) techniques for modelling LST. LSMA derived biophysical parameters corresponded more strongly to LST than those produced using index-based parameters. Results indicated that vegetation and water surfaces had relatively stable LST but it increased by around 2 ℃ when these surfaces were converted to built-up areas with extensive impervious surfaces. Knowledge of the expected change in LST when one land-cover is converted to another can inform land planners of the potential impact of future changes and urges the development of better management strategies.

Keywords: LULC; LST; urban thermal environment; emissivity; surface urban heat islands

1. Introduction

Over the last two decades, the rate of urbanisation on a global scale has been explosive, increasing from 12% in 1990 [1] to over 50% in 2011 [2]. This meteoric rise has generally emerged from high population growth [3] and rural to urban migration, both of which have been rapid in developing countries due to inadequate planning guidelines and the pursuit of economic development [4]. Of the world's developing countries, those within Asia are experiencing the highest rate of urban growth [2]. In particular, Dhaka Megacity, Bangladesh, is one of the fastest growing cities in the world [5,6].

The population in Dhaka Megacity (hereafter Dhaka) has increased from 2.3 million in 1975 [7] to approximately 15.4 million in 2011 [2]. Failure to manage urban growth has led to a significant decline in urban green space over this time, with natural surfaces rapidly being converted into impervious ones [8,9]. Extensive removal of natural surfaces modifies heat retention, its dispersion and evaporative and transvaporative rates [10], which in-turn modifies local climate, air flow and atmosphere [11,12]. Combined, these factors can create an urban heat island (UHI) effect, where urban atmospheric and surface temperatures become significantly warmer than its natural surrounds [11,13].

UHIs have a profound impact on human well-being due to temperature driven increases in infectious diseases [14,15] and have potential to contribute to increasing dengue fever [16] and typhoid fever [17] risk in Dhaka. Considering that Dhaka has been found to have experienced significant urban green space and floodplain removal over the last several decades due to urban development [5,9,18] and its influence on UHI formation, it is vital that modification to Dhaka's urban thermal environment over a multi-decadal period is better understood.

Traditional urban thermal environmental studies are based on the collection of air temperature readings at multiple locations between urban and rural landscapes from weather stations [19], mobile thermometers [20] or both [21]. These approaches are somewhat limited in developing cities where weather stations are unavailable or infrequent [22], such as in Dhaka. Remotely sensed (RS) imagery can be an alternative source for studying urban thermal environments via the analysis of land surface temperature—LST. Through LST, the surface urban heat island (SUHI) effect can be studied, and based on strong relationships observed between near surface air temperature and LST, is considered a reliable indicator of atmospheric UHIs [23,24]. Imagery acquired from the Landsat series of satellites have been the most commonly used medium for assessing changes to urban thermal environments arising from land-use/land-cover (LULC) modification [25-27].

Two common approaches to investigate the relationship between LULC and LST are recognised [24]. One approach utilises information recorded from multispectral sensors to determine and compare LST of various LULC types over multiple dates [28]. The other approach is to extract biophysical parameters that quantitatively represent various LULC types from multispectral imagery through the use of indices or classification routines, and utilise these parameters to model LST [24]. Common indices and classification routines include: the Normalised Difference Vegetation Index (NDVI) to highlight vegetated surfaces [29]; the Normalised Difference Built-up Index (NDBI) for urban built-up surfaces [30]; the Modified Normalised Difference Water Index (MNDWI) for water body detection [24]; and linear spectral mixture analysis (LSMA) [31].

LSMA has seen increased use in urban thermal studies due to its ability to consider the mixed-pixel problem inherent in multispectral imagery [32]. This process separates multispectral image pixels into multiple 'fraction' images that represent the relative abundance of materials captured in multispectral imagery based on its spectral characteristics [33,34]. Fraction images in this approach include the Green Vegetation Fraction - GVF and Impervious Surface Area—ISA fraction [32]. Here, we extend on this approach by applying it to multi-date Landsat imagery.

This study uses multi-date Landsat imagery (1990-2000-2011) to explore the consequences of rapid LULC modification resulting from rapid urbanisation on LST in Dhaka. Specifically, we aim to: (a) calculate LST for all three dates and compare it to contemporaneously mapped LULC; and (b) calculate biophysical parameters using index-based and linear spectral unmixing (fraction based) and assess their utility for LST modelling. We hypothesise that the greatest change in LST will be coincident to areas that have been converted into impervious surfaces as a consequence of

rapid urbanisation and that fraction-based imagery will provide superior results, relative to an index-based approach, due to its ability to unmix land-covers from pixels.

2. Study area

The study area is focused on Dhaka, Bangladesh (Figure 1). The broad Dhaka metropolitan extent is commonly referred to as Dhaka Megacity (DM), which is based on population number as defined by the Bangladesh Bureau of Statistics (BBS) in 1991. As access to urban planning and development spatial data is limited in Bangladesh, the official entirety of the DM could not be considered. Instead, a bounding polygon that includes a subset of both the DM and Dhaka Metropolitan Development Plan (DMDP) planning area zone (as defined by the City Development Authority, RAJUK) was used. Inclusion of the DMDP extended the DM study area extent along its east and southeast boundary only—the north, south and west DMDP extent falls entirely within the DM [9]. The study area covers an area of approximately 87,400 ha, and comprises the Tongi, Savar and Keraniganj municipalities in the northern, western and southern areas of the study area, respectively (Figure 1).

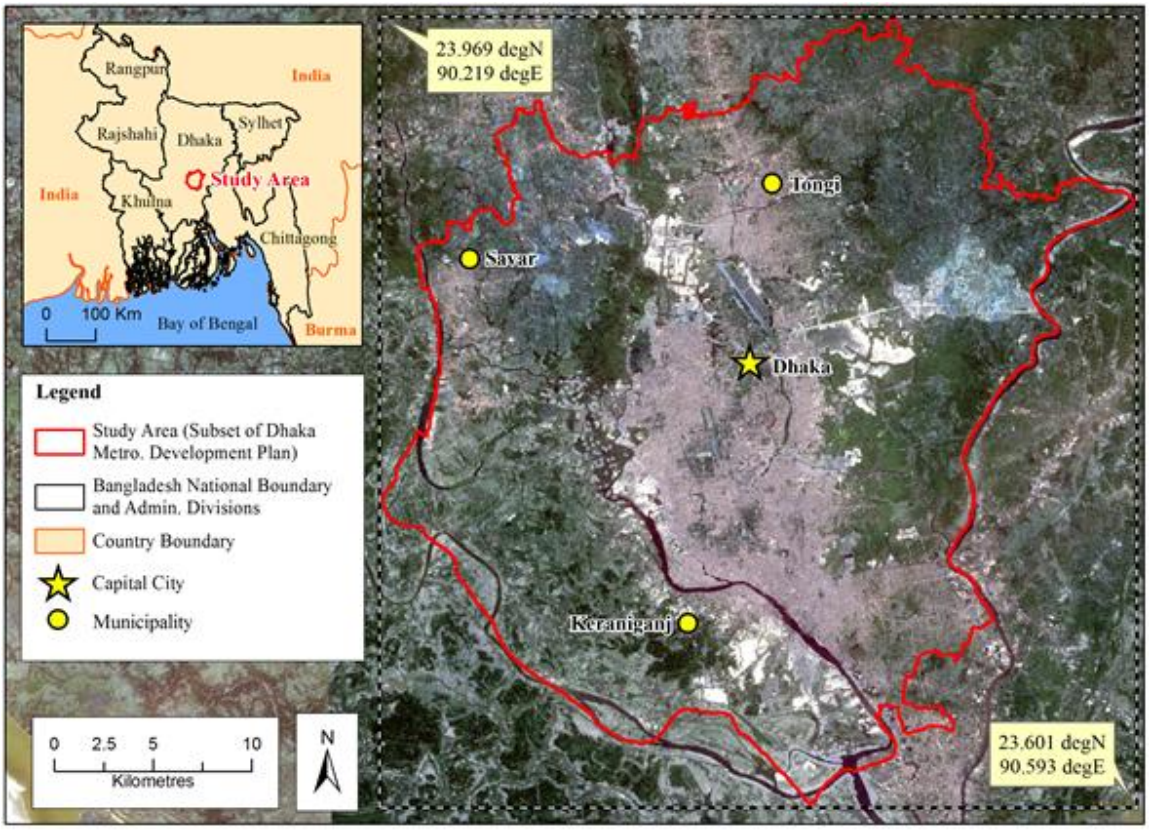

Figure 1. Location of study area (Dhaka) in the context of the Dhaka Metropolitan Development Plan and Bangladesh National Boundary.

Dhaka is situated on the eastern banks of the Buriganga River and lower reaches of the Ganges Delta on flat low-lying land close to sea level [8]. It experiences a humid, hot and wet subtropical climate with an annual mean temperature of 26.1 °C [35]. Three broad seasons are recognised; a cool and dry winter from November to February, a hot and dry summer from March to May, and a rainy monsoon season from June to October [9,36].

3. Materials

3.1. Image selection and pre-processing

Three Landsat 5 TM (Thematic Mapper) images captured on 7 January 1990 at 10:00 AM Bangladesh Time (BDT) (late winter), 8 March 2000 at 10:30 AM BDT (early summer), and 4 April 2011 10:30AM BDT (peak summer) were acquired from the Geo-Informatics and Space Technology Development Agency (GISTDA), Thailand. As the study area is on the boundary of two Landsat Rows, two scenes were acquired for each year, located at row/path 137/43 (northern scene) and 137/44 (southern scene). All bands have a spatial resolution of 30 m except for band 6 - thermal infrared (TIR) with a resolution of 120 m. All Landsat images were provided at Level 1G, which are corrected for radiometric geometrical distortions.

3.1.1. Geometrical correction

All Landsat scenes were subjected to further geometrical correction using 75 ground control points (GCPs) taken from topographic maps of 1990 to register each scene to the Bangladesh Transverse Mercator (BTM) system [37]. The selected GCPs were well dispersed throughout scenes and resulted in a root-mean-square-error (RMSE) of <0.5 of a pixel using a first-order polynomial and nearest-neighbour resampling.

3.1.2. Calibration and atmospheric correction

The raw digital numbers (DNs) for each Landsat 5 image (bands 1-5,7) were first converted to at-sensor spectral radiance by applying the calibration coefficients (gains and bias) specified by Chander and Markham [38] and Chander et al. [39]. This process used an image-based radiometric correction [40] to minimise radiometric differences between images and was applied using the COST model in IDRISI Selva [41] via the following formula:

$$L_s = gain * DN + bias \quad (1)$$

where L_s represents at-sensor spectral radiance in Watts * m^{-2} * sr^{-1} * μm^{-1}, *gain* and *bias* are conversion coefficients, and *DN* is the digital number [40]. The COST model then removed atmospheric effects arising from changes in surface reflectance [39,40] using various atmospheric parameters including image capture date (in GMT) and sun elevation angles obtained from Landsat header files, and DN haze values derived from blackbody pixels and band wavelengths.

This process was undertaken to ensure the cosine effect of different solar zenith angles due to time differences between image capture, exo-atmospheric solar irradiance differences due to aerosols and dust particles, and variation arising from sun-to-earth distance differences were corrected [38,39,41]. COST achieves this with the following formula:

$$\rho_\lambda = \frac{\pi * L_\lambda * d^2}{\mathrm{ESUN}_\lambda * \cos\theta s} \quad (2)$$

where ρ_λ represents unit-less planetary reflectance, L_λ is spectral radiance, d^2 is earth-sun distance in astronomical units squared, and ESUN_λ is mean solar exo-atmospheric irradiances.

Finally, the pairs of Landsat scenes were mosaicked into a single image for each study year and

clipped to the study area boundary. The resulting atmospherically corrected images were used to derive biophysical parameters. Calibration and correction of Landsat 5 TIR imagery (band 6) during LST calculation is outlined in Section 4.1.

3.2. Land-use/Land-cover

LULC images for 1990, 2000 and 2011 are shown in Figure 2. These images were provided by Dewan and Corner [9], who developed several LULC images of the study area with classes based on a modified Anderson Level 1 Scheme [42] and derived via a hybrid classification technique as outlined by [43]. Subsequent accuracy assessment performed by Dewan and Corner [9] indicated an overall accuracy of 88%, 90% and 95% for the 1990, 2000 and 2011 LULC images, respectively. Preliminary assessment of the LULC images suggest that built-up and bare-soil surfaces are located predominately within Dhaka's central urban core and have expanded to the north and south over the study period. Floodplains almost completely surround the central urban core on all sides. It is from the close proximity of these floodplains that Dhaka experiences considerable flooding during rainy season periods [5] and highly fertile soils [44].

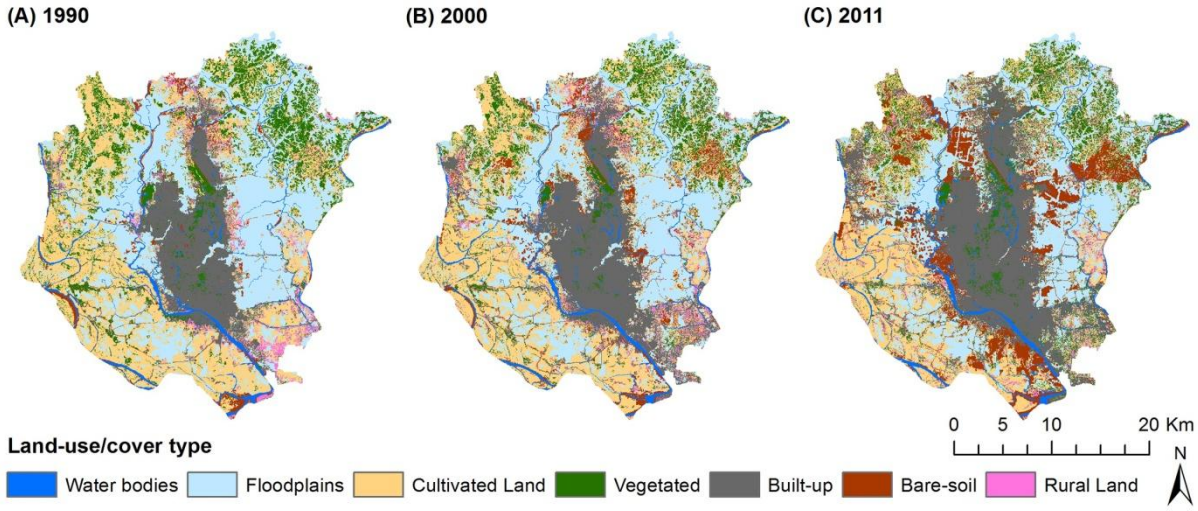

Figure 2. Land-use/land-cover types found in the study area in (A) 1990, (B) 2000 and (C) 2011 (after Dewan and Corner [9]).

4. Methods

4.1. Calculation of LST

Several methods exist for deriving LST from the Landsat 5 TIR band (band 6), including the mono-window routine (45) and single-channel algorithm (46). These methods require ancillary atmospheric information and parameters over the study area during satellite overpass to compensate for atmospheric differences between Landsat images. As atmospheric information was unavailable for all Landsat image capture dates, an alternative image-based approach was employed to derive LST based on 47, 48 and 49.

First, the DN of each TIR band was converted to spectral radiance (L_s) derived using Equation 1 [40] and then transformed to at-sensor brightness temperature (T_s) through the inverted Planck's law (Equation 3) using calibration constants obtained from Chander et al. [39]:

$$T_s = \frac{K_2}{\ln\left(\frac{K_1}{L_s}+1\right)} \tag{3}$$

where T_s is the effective at-sensor brightness temperature in Kelvin (K), L_s is the spectral radiance at the sensor's aperture in Watts * m^{-2} * sr^{-1} * μm^{-1}, and K_1 and K_2 are calibration constants. For Landsat 5 TM satellite, K_1 = 607.76 Watts * m^{-2} * sr^{-1} * μm^{-1} and K_2 = 1260.56 K, respectively.

Secondly, the derived T_s images were then corrected for spectral emissivity [50] using the NDVI Threshold Method proposed by Sobrino et al. [51]. This method was chosen as it is considered appropriate for the estimation of emissivity for Landsat TM data as multiple thermal bands and night-time images are not required, unlike other methods such as temperature and emissivity separation (TES) and thermal infrared spectral indices (TISI) [27]. Furthermore, use in LST studies has proven successful [52,53].

The NDVI threshold method obtains the emissivity values from an NDVI image by considering three different cases, based on fixed thresholds: soil pixels (NDVI < 0.2), pixels of dense vegetation (NDVI > 0.5) and pixels with mixed soil and vegetation (0.2 ≤ NDVI ≤ 0.5). To convert NDVI values into land surface emissivity, the emissivity coefficient (ε) was set to 0.96 for soil pixels ($\varepsilon = \varepsilon_{S\lambda}$) and 0.99 for dense vegetation pixels ($\varepsilon = \varepsilon_{V\lambda} + C_\lambda = 0.985 + 0.005$) based on Artis and Carnahan [50], Nichol [54] and Sobrino et al. [55]. The emissivity coefficient for mixed soil and vegetation pixels was calculated using Equation 4 [55] where P_{vege} is the vegetation fraction obtained according to Equation 5 [56] and the cavity effect (C_λ), which accounts for effects of rough or heterogeneous surfaces, was calculated using Equation 6 with a geometrical factor (F') set to 0.55 after Sobrino et al. [57].

$$\varepsilon = \varepsilon_{V\lambda} * P_{vege} + \varepsilon_{S\lambda} * (1 - P_{vege}) + C_\lambda \tag{4}$$

$$P_{vege} = \left(\frac{NDVI - NDVI_{soil}}{NDVI_{vege} - NDVI_{soil}}\right)^2 \tag{5}$$

$$C_\lambda = (1 - \varepsilon_{S\lambda}) * \varepsilon_{V\lambda} * (F') * (1 - P_{vege}) \tag{6}$$

In addition, a value of 0.955 was used for surface water emissivity and all major water-bodies were masked out of the Landsat imagery, as water can influence the accuracy of the process [58].

Lastly, land surface temperature (LST) was retrieved from the T_s imagery and atmospherically corrected emissivity data. This used a method proposed by Artis and Carnahan [50], which is suited to studies that lack ancillary atmospheric parameters [32,47,49]:

$$\text{LST} = \frac{T_S}{1 + \left(\frac{\lambda \sigma T_B}{hc}\right)\ln\varepsilon} \tag{7}$$

where T_s is the derived brightness temperature, λ is the effective wavelength (11.475 μm for Landsat TM band 6), σ is Boltzmann constant (1.38×10^{-23} J/K), h is Planck's constant (6.626×10^{-34} J_s), c is velocity of light in a vacuum (2.998×10^{-8} m/s), and ε is the atmospherically corrected emissivity value. As the LST images represent different years and seasons, LST images were finally normalised using the method suggested by Carlson and Arthur [59].

4.2. Calculation of biophysical parameters

4.2.1. Index-based approach

The use of index-based biophysical parameters in LST analysis and modelling can provide important insight into the heat mitigation or enhancement characteristics of various land surfaces [60,61]. Indices used in this study include NDVI to highlight densely vegetated surfaces [62], the NDBI (normalised difference built-up index) as an indicator of built-up urban surfaces and bare-soil [30], and the MNDWI (modified normalised difference water index) as an indicator of water-bodies and rivers [63]. The NDVI, NDBI and MNDWI indices (Equation 8-10, respectively) were calculated using ArcMap 10.1 [64].

$$\text{NDVI} = \frac{R_{NIR} - R_{RED}}{R_{NIR} + R_{RED}} \tag{8}$$

$$\text{NDBI} = \frac{R_{MIR} - R_{NIR}}{R_{MIR} + R_{NIR}} \tag{9}$$

$$\text{MNDWI} = \frac{R_{GREEN} - R_{MIR}}{R_{GREEN} + R_{MIR}} \tag{10}$$

where R_{NIR} is the reflectance in the near-infrared band (TM band 4), R_{RED} and R_{GREEN} are the reflectance in red and green bands (TM band 3 and 2, respectively), and R_{MIR} is the reflectance in the middle infrared band (TM band 5).

4.2.2. Linear spectral mixture analysis

An alternative to index-based biophysical parameters is linear spectral mixture analysis (LSMA), which is able to unmix the components within a pixel [65]. LMSA was used to derive the green-vegetation fraction (GVF), which is similar to NDVI and estimates the fraction of green vegetation within each pixel. The impervious surface abundance (ISA) fraction, which is similar to the NDBI, estimates the fraction of built-up or bare-soil surfaces per pixel. LSMA was completed in two main stages using ENVI 4.8 software [66].

Stage 1: Water-body masking and image normalisation

Pixels representing water are typically masked-out prior to undertaking LSMA as these pixels add unnecessary endmember spectra into the spectral range [32]. A unique mask was created from the water class of each LULC map. Wu [67] indicates that it is beneficial to reduce brightness variability within each fraction image to reduce the number of endmembers representing each component, thus reducing redundant information whilst retaining useful information for separating vegetation, impervious surface and soil fractions. To achieve this, the Normalised Spectral Mixture Analysis (NSMA) method [67] was implemented for each Landsat scene. The NSMA method uses the following equations based on Wu [67]:

$$\acute{R}_b = \frac{R_b}{\mu} \times 100 \tag{11}$$

$$\mu = \frac{1}{N}\sum_{b=1}^{n} R_b \tag{12}$$

where $\acute{R}_b$ is the normalised reflectance for Landsat 5 TM band b in a pixel, R_b is the original reflectance for Landsat 5 TM band b, μ is the average reflectance for that pixel, and N is the total number of Landsat 5 TM bands (i.e., 6 bands for Landsat TM).

Stage 2: Minimum noise fraction transform, pixel purity index and n-dimensional visualisation

Landsat image dimensionality was reduced to remove unnecessary noise from image bands by using the Minimum Noise Fraction (MNF) transform. The MNF comprises of two standard principal component (PC) transforms, which provide an output composed of uncorrelated MNF components that are used to assist in the endmember selection process [68]. We used the first four components in LSMA as the other components were comprised of noise. Following this, pure-pixel endmembers were identified by refining the MNF components and mixed pixels via a Pixel Purity Index (PPI) algorithm [69,70]. The endmembers trialed for each Landsat scene included: vegetation, soil, and impervious surface.

After selection of endmembers, the constrained least-squares solution (Equation 13) was applied to unmix the MNF components identified earlier in which the residual e_b is minimized:

$$\acute{R}_b = \sum_{i=1}^{m} \acute{f}_i \, \acute{R}_{i,b} + e_b \tag{13}$$

where $\acute{f}_i$ is the fraction of endmember i, $\sum_{i=1}^{m} \acute{f}_i = 1$ and $\acute{f}_i = \geq 0$; $\acute{R}_{i,b}$ is the normalised reflectance of endmember i in band b for that pixel; m is the number of endmembers; and e_b is the residual or band error. Additionally, the constrained least-squares solution assumes (Equation 14):

$$\text{RMSE} = \sqrt{\frac{\left(\sum_{i=1}^{m} e_i^2\right)}{m}} \tag{14}$$

This approach unmixed the selected MNF components into Green Vegetation Fraction (GVF), Impervious Surface Area (ISA), and soil abundance fraction images, and a summary of root-mean-square-error (RMSE) statistics was produced (Table 1).

Table 1. Summary of root-mean-square-error (RMSE) statistics derived from linear spectral mixture analysis for combinations of three (vegetation, soil, impervious surface) endmembers for each study year.

RMSE	1990	2000	2011
Minimum	0.00	0.00	0.01
Maximum	0.23	0.34	0.29
Mean	0.11	0.17	0.21

4.3. Temporal comparison of LULC to LST

Spatial relationships, patterns and distributions between LULC classes and LST over the study period were visualised and explored by overlaying each LST images over their corresponding LULC classes map using ArcMap 10.1. The mean LST of each LULC type for each year was obtained using Zonal Statistics. Significant differences ($\alpha = 0.05$) between the LST means of each LULC class across years were then determined using Tukey's Honestly Significant Different test [71] to explore potential changes to Dhaka's urban thermal environment over the study period. Image differencing was undertaken on LULC class maps to generate change maps for the periods: 1990–2000, 2000–2011, and 1990–2011, which were then linked to LST images as tables to explore influence of LULC change on LST.

Variation in LST is the result of several factors including LULC change, time of the day, and seasonality [11,72]. All acquired Landsat images used in analysis were captured at the same approximate time (10:00 AM Bangladesh local time) due to the sun-synchronous orbit [73], avoiding acquistion time issues. To correct for differences in seasonality, the normalisation method developed by Zhou and Wang [24] was utilised to correct seasonal differences in LST whilst retaining differences in LULC type. This approach compares the mean LST of each LULC type across each image using the following equations (Equation 15–17):

$$dT_{ij} = T_{j(Ya)} - T_{i(Yb)} \tag{15}$$

$$\Delta T_i = T_{i(Ya)} - T_{i(Yb)} \tag{16}$$

$$dT_n = dT_{ij} - \Delta T_i \tag{17}$$

where dT_{ij} is the temperature difference between LULC type j in the first comparison year (Y_a) and LULC type i in the second comparison year (Y_b); ΔT_i is the temperature difference for the same LULC type i between two comparison years; dT_n is the normalised temperature by subtracting $dT_{ij} - \Delta T_i$.

4.4. Comparison of LST and biophysical parameters

Relationships were examined between LST images and biophysical parameters at 1000 samples distributed randomly over the entire study area. Samples were generated using a stratified random sampling design, where 148 random samples were randomly generated for each of the LULC strata. The strength of the relationship between biophysical parameters and LST was examined using univariate regression via SPSS Statistics software [74]. Fisher's r to z transformation [75] was used to identify if the correlation between LST and LMSA were significantly different to the index-based parameters (i.e., NDVI vs GVF; NDBI vs ISA).

5. Results

5.1. Temporal comparison of LULC to LST

High LST areas were observed to be associated with built-up and bare-soil LULC classes, based on a visual comparison between Figure 2 and Figure 3. In contrast, areas of lower LST are associated with floodplains, cultivated land and vegetation. Figure 3 indicates that surface temperature is increasing in both magnitude and spatial distribution over time.

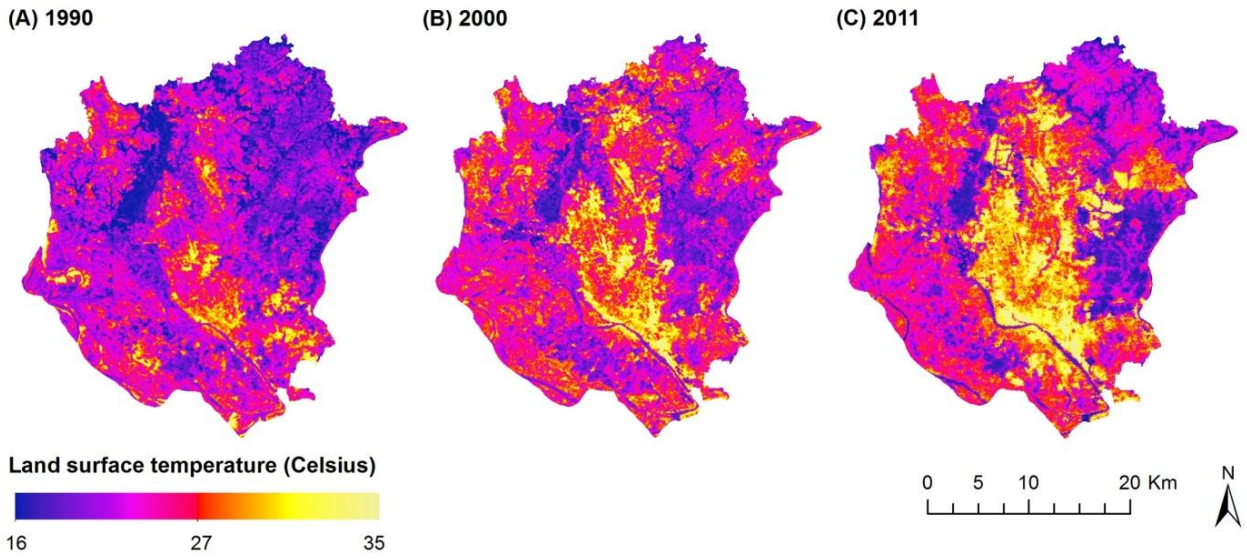

Figure 3. Land surface temperature of the study area in: (A) 1990; (B) 2000; and (C) 2011.

Locations with high NDVI and GVF values (Figure 4), and thus densely vegetated, declined significantly over the study period, particularly in Dhaka's central urban core (Figure 4). In contrast, locations with high NDBI and ISA values increased, indicating urban development over the study period. Locations with high MNDWI values declined on floodplain areas over the study period. These trends, in particular decreasing vegetated surfaces due to conversion into impervious surfaces, have been noted in Dhaka in similar studies [76,77].

Built-up, bare-soil and cultivated LULC types consistently exhibited the highest mean LST, which increased significantly at each temporal data point studied (Table 2). In contrast, water-bodies consistently exhibited the lowest temperatures each year and did not significantly change throughout the study period when using normalised LST imagery. Floodplains and vegetated land maintained low LST and did not change significantly between 2000 and 2011 (Table 2). Comparison of each year indicated that the mean LST of each LULC type continually increased over the study period and these changes were significant between years for built-up areas, bare-soil, cultivated and rural classes, with the greatest mean increases occurring in the built-up and bare-soil classes. Comparison between water LULC types using normalised and non-normalised LST images was undertaken to explore the influence of seasonality on surface temperature. While water LST is considerably consistent and not significantly different across study years, water temperature based off non-normalised imagery increases considerably across years and present LST means that are significantly different.

Influence of LULC type on LST modification was explored by subtracting LST values for each LULC type for the periods 1990 to 2000 and 2000 to 2011 (Table 3). This was undertaken for both normalised and non-normalised LST images as a consideration for potential seasonal differences between LULC types. Investigation of normalised LST for the two periods indicates that LST increased markedly when natural LULC types were converted into built-up and bare-soil. Not surprisingly, water-bodies exhibited the highest LST increase when converted into built-up areas, with an average increase of *ca.* 2 °C (Table 3). Similarly, mean LST for vegetated surfaces and floodplains increased by an average of *ca.* 1.2 °C and 1.6 °C, respectively, when converted into impervious surfaces (Table 3). These temperature increases align with similar studies, which have

noted an LST increase over 2 °C following the conversion of vegetated surfaces into impervious or bare-soil following urban developments over several decades in similar climates [78,79].

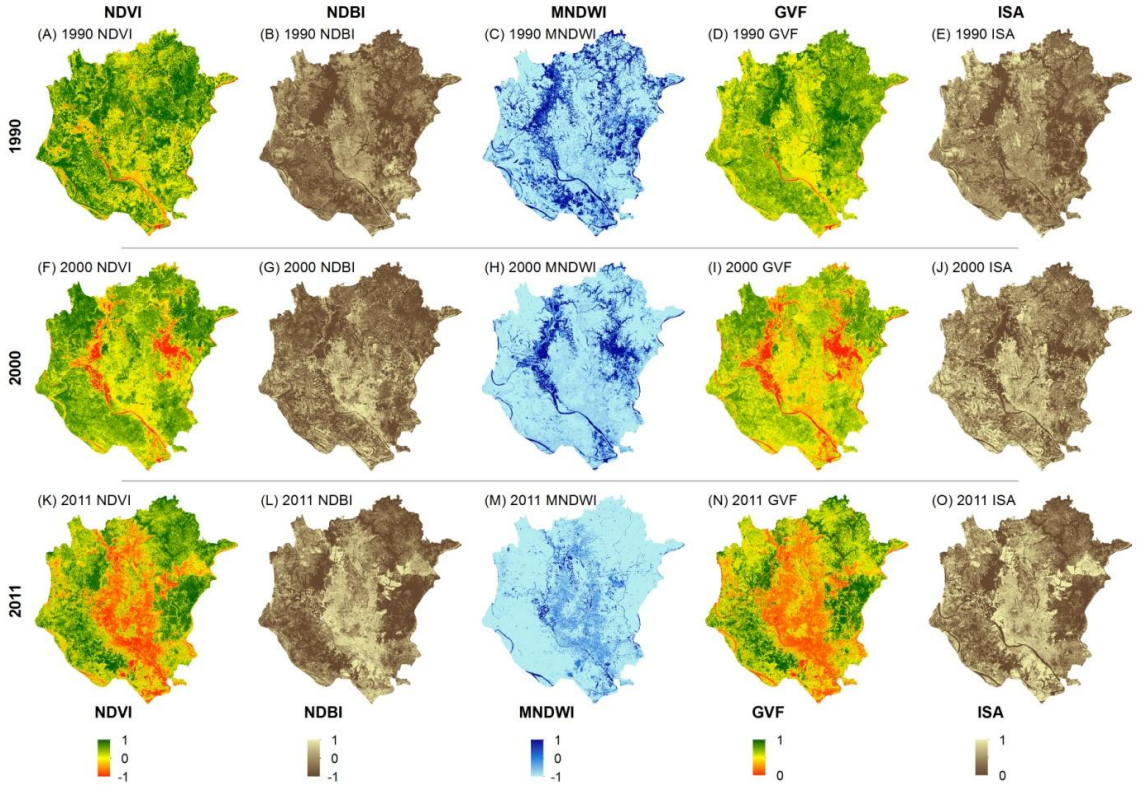

Figure 4. Spatial distribution of NDVI (A, F, K), NDBI (B, G,L), MNDWI (C, H, M), GVF (D, I, N) and ISA (E, J, O) biophysical parameters for the three time points studied (see text for a description of the acronyms).

Table 2. Mean land surface temperature showing the variability of each land-use/land-cover over the study period.

LULC Type	Land Surface Temperature (°C)						
	1990		2000		2011		All Years
	Mean[a]	SD[b]	Mean	SD	Mean	SD	Mean
Built-up	21.18[a]	1.03	25.36[b]	1.03	27.69[c]	1.38	24.74
Bare-soil	20.79[a]	1.31	24.86[b]	1.07	27.38[c]	1.51	24.34
Cultivated	20.56[a]	1.05	24.32[b]	0.67	25.76[c]	0.99	23.55
Rural	20.47[a]	1.01	24.25[b]	0.67	25.85[c]	1.04	23.52
Vegetated	19.12[a]	0.85	23.15[b]	0.57	24.11[b]	1.03	22.13
Floodplain	19.01[a]	1.06	23.24[b]	0.81	23.74[b]	1.11	22.00
Water (N*LST*[c])	18.24[a]	0.91	18.53[a]	0.71	18.91[a]	1.46	18.56
Water (Non-N*LST*[d])	18.56[a]	1.03	23.09[b]	0.93	24.47[c]	0.75	22.04

[a] Different subscripts represent significantly different LST means ($\alpha = 0.05$) between years for land-use/land-cover type;

[b] SD = Standard Deviation

[c] N*LST* = Normalised land surface temperature

[d] Non-N*LST* = Non-normalised land surface temperature.

The LST of cultivated land resulted in only minor change when converted into built-up and bare-soil for both comparison periods. Likewise, temperature differences between built-up and bare-soil were minimal (Table 3).

Considering that the greatest LST change appears to be associated with natural areas being converted into impervious surfaces, built-up and bare-soil classes were merged to further explore the spatial correspondence between LST and LULC change due to urbanisation. Floodplains, cultivated land and vegetation were not included due to seasonal influence. Comparison between each of the time periods indicates that impervious surfaces have expanded on to surrounding LULC types such as floodplains, water-bodies and cultivated land (Figure 5). Likewise, urban expansion appears to be moving from the urban core in north, north-east, north-west, east, and south-east directions.

Table 3. Influence of land-use/cover change on non-normalised and normalised land surface temperature for 1990–2000 and 2000–2011 comparison periods. No LULC occurred in classes with the same label.

Land-use/cover Type		Land Surface Temperature (^{o}C)					
		Comparison Period					
		1990–2000			2000–2011		
Converted From	To	Non-Norm. *dT*[a]	Non-Norm. *dT* (SD[b])	Norm. *dT*[c]	Non-Norm. *dT*	Non-Norm. *dT* (SD)	Norm. *dT*
Water	Water	4.53	4.2	0.28	1.38	3	0.3
	Floodplain	3.74	2.5	0.5	0.71	4.1	0.79
	Culti. land	4.32	2.5	0.96	2.23	3.8	0.81
	Vegetated	4.04	1	0.59	2.33	0.7	0.49
	Built-up	5.36	0.0	2.18	4.78	2.2	2.03
	Bare-soil	4.66	2.2	1.59	3.66	0.4	1.13
	Rural	4.25	0.3	0.47	2.33	4.2	0.28
Floodplain	Water	5.03	0.2	0.5	2.17	1.5	0.79
	Floodplain	4.24	1.8	0.0	1.5	0.7	0.0
	Culti. land	4.82	3.4	1.06	3.02	0.5	0.57
	Vegetated	4.54	0.8	0.59	3.11	3.1	0.3
	Built-up	5.86	2.3	1.68	4.95	0.5	1.62
	Bare-soil	5.16	2.2	1.09	4.44	4.8	0.92
	Rural	4.75	0.9	0.97	3.11	2.4	0.51
Cultivated Land	Water	3.97	3	−0.96	1.59	2.7	−0.81
	Floodplain	3.18	3.3	−1.06	0.93	2.2	−0.57
	Culti. land	3.76	2.4	0.0	2.44	1.2	0.0
	Vegetated	3.49	3.9	−0.46	2.54	3.1	−0.27
	Built-up	4.8	2	0.63	4.37	3.2	1.05
	Bare-soil	4.1	0.8	0.03	3.87	2.1	0.34
	Rural	3.69	4.1	−0.09	2.54	4.9	−0.07

Continued on next page.

Vegetated	Water	4.44	0.4	0.59	1.86	1	0.49
	Floodplain	3.65	1.2	−0.59	1.2	2.7	−0.3
	Culti. land	4.22	0.8	0.46	2.72	0.4	0.27
	Vegetated	3.95	3	0.0	2.81	3.8	0.0
	Built-up	5.27	2.3	1.09	4.64	1.5	1.32
	Bare-soil	4.57	2.8	0.75	4.14	1.1	0.62
	Rural	4.15	1.5	0.37	2.81	3.3	0.21
Built-up	Water	3.35	1.9	−2.18	0.55	3.8	−2.03
	Floodplain	2.56	0.2	−1.68	−0.12	4.8	−1.62
	Culti. land	3.13	2.3	−0.63	1.4	0.8	−1.05
	Vegetated	2.86	2.8	−1.09	1.49	0.4	−1.32
	Built-up	4.18	3.5	0.0	3.33	1.4	0.0
	Bare-soil	3.48	2	−0.59	2.82	0.3	−0.7
	Rural	3.06	3.2	−0.72	1.49	0.5	−1.11
Bare-soil	Water	3.94	3.5	−1.59	1.25	1.6	−1.13
	Floodplain	3.15	2.4	−1.09	0.58	3.2	−0.92
	Culti. land	3.73	1.1	−0.03	2.1	2.1	−0.34
	Vegetated	3.45	2.9	−0.75	2.2	3	−0.62
	Built-up	4.77	1.3	0.59	4.03	3.8	0.7
	Bare-soil	4.07	4.6	0.0	3.53	1.1	0.0
	Rural	3.66	1.9	−0.12	2.2	1.4	−0.41
Rural	Water	4.06	1.2	−0.47	1.66	2.3	0.28
	Floodplain	3.27	1.5	−0.97	0.99	3.3	−0.51
	Culti. land	3.85	4.2	0.09	2.51	0.3	0.07
	Vegetated	3.58	4.4	−0.37	2.61	3	−0.21
	Built-up	4.89	0.3	0.72	4.44	2.5	1.11
	Bare-soil	4.19	3.5	0.12	3.94	0.8	0.41
	Rural	3.78	2.2	0.0	2.61	1.9	0.0

[a] Non-norm. *dT* = Non-normalised land surface temperature difference;

[b] Norm. *dT* = Normalised land surface temperature difference;

[c] SD = Standard Deviation.

Differences in LST were calculated and visualised for the comparison periods in order to inspect the influence of urban development on LST change (Figure 6). Differences in LST across study periods were also calculated and visualised to assess LST changes as a result of LULC modification (Figure 6). The thermal environment of Dhaka matched these cover changes across each comparison period, with significant expansion of LST into areas that were floodplains and rural land that have changed into impervious, built-up, areas (cf. Figure 5 and Figure 6).

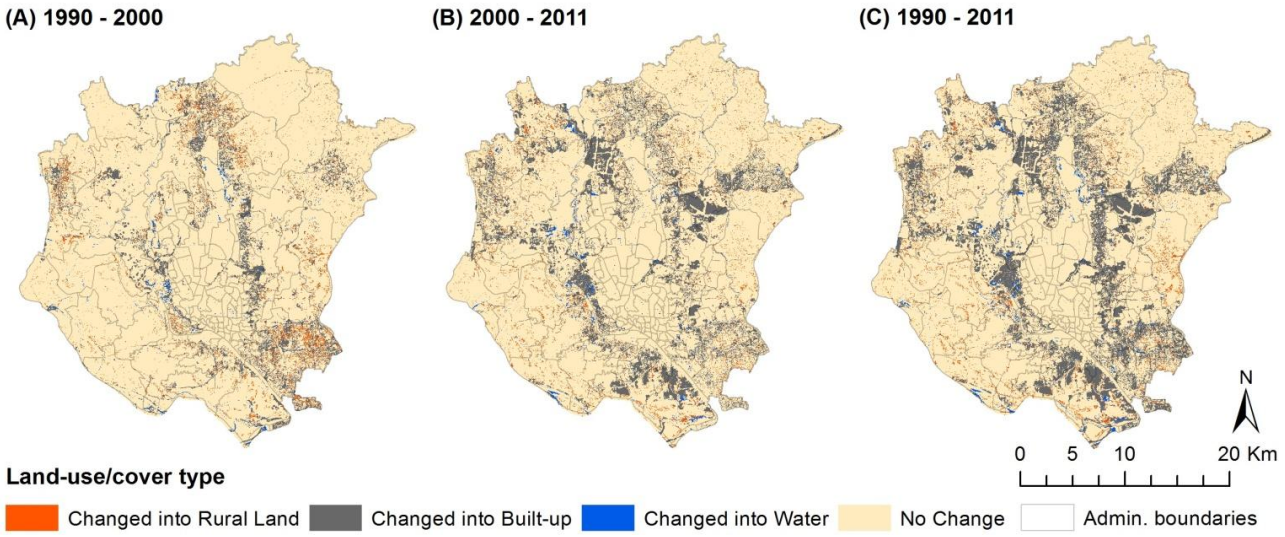

Figure 5. Land-use/cover conversion into Built-up, Rural Settlements and Water-body for (A) 1990–2000, (B) 2000–2011 and (C) 1990–2011.

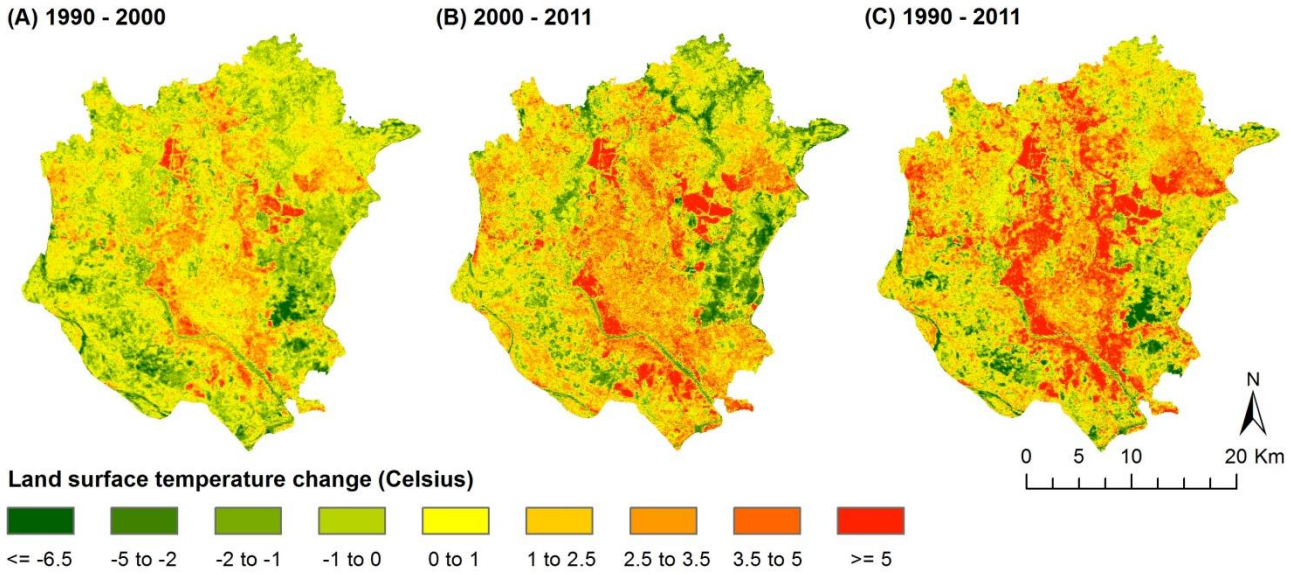

Figure 6. Land surface temperature differences for (A) 1990–2000; (B) 2000–2011; and (C) 1990–2011.

5.2. Comparison of LST and biophysical parameters

The strength of the correlation between NDVI/GVF and LST varied considerably between years (Figure 7), although it was persistently negative, reflecting the inverse relationship often observed between dense vegetation and LST. In contrast, the correlation between NDBI/ISA and LST was positive, strong, and relatively stable throughout the study period highlighting LST increases in tandem with impervious surfaces (Figure 7) These trends, particularly those between vegetation, impervious surfaces and LST, have been highlighted in similar studies [12,60]. The MNDWI consistently had a weak negative correlation with LST for the study period (Figure 7 G,H,I), indicating the resistance of water-bodies to increases in LST.

Comparison of the correlation coefficients between the fraction-based approach (GVF) and the index-based approach (NDVI) for detecting greenness identified that the GVF was a better predictor of LST than the NDVI. However, differences were only significant in 1990 (Table 4). Likewise, the ISA fraction-based approach had consistently higher correlation with LST than the NDBI for all time periods, although differences were not significant at $\alpha = 0.05$ (Table 4). Within techniques, the NDBI was significantly more correlated to LST than NDVI (1990-2000) and the ISA outcompeted the GVF (Table 4).

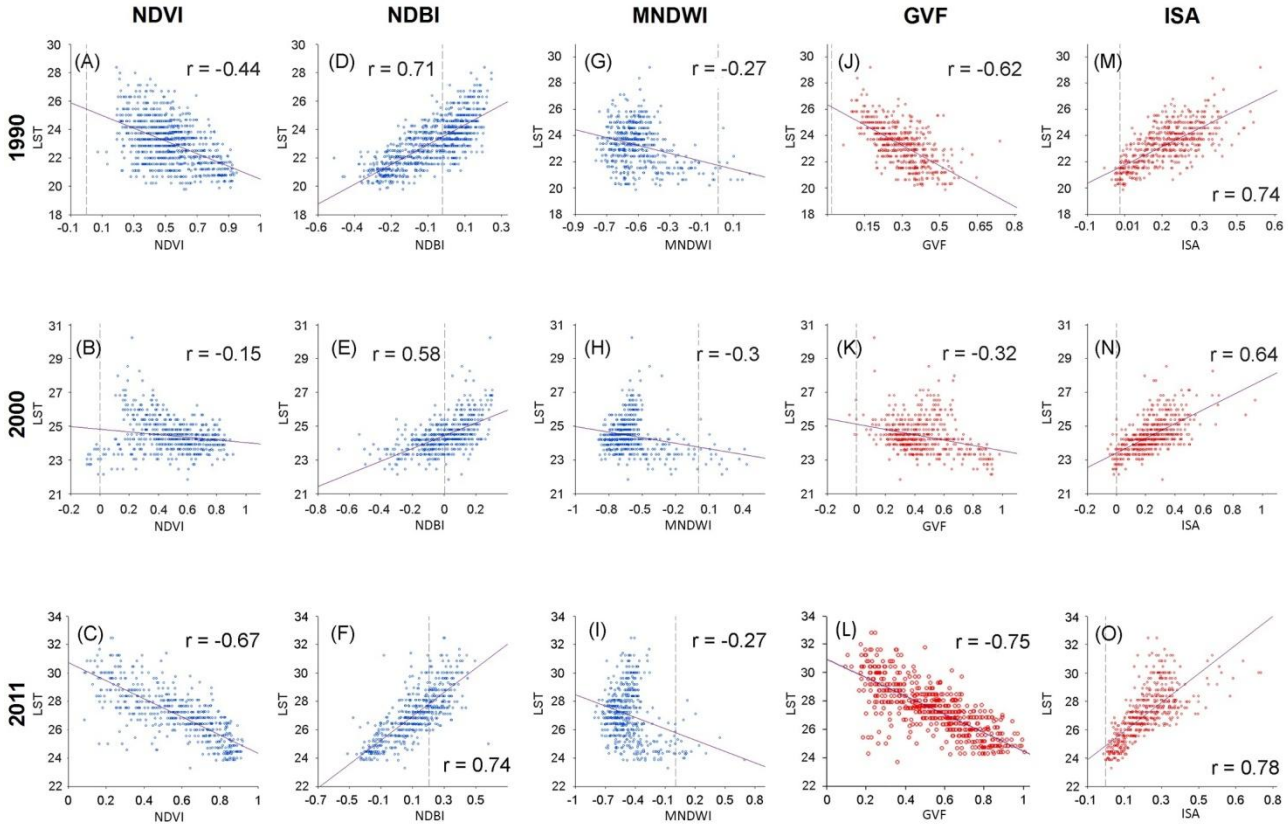

Figure 7. Visualisation of univariate regression scatter-plots between land-surface temperature and NDVI, NDBI, MNDWI (blue), GVF and ISA (red) biophysical parameters over the study period (see text for a description of the acronyms). The dashed vertical line represents 0 units.

Table 4. Significant differences between the corresponding index-based and fraction-based approaches (i.e., NDVI vs GVF; NDBI vs ISA).

	NDVI vs GVF[1]	NDBI vs ISA	NDVI vs NDBI	GVF vs ISA
1990	0.04	0.33	<0.05	0.06
2000	0.10	0.25	<0.05	<0.05
2011	0.13	0.25	0.17	0.31

[1]*p*-values < 0.05 identify significant differences between approaches.

6. Discussion

Dhaka's urban thermal environment has been significantly modified over the last several decades as a result of LULC change from rapid urbanisation. Built-up and bare-soil surfaces associated with urban growth have rapidly replaced pre-existing natural surfaces including vegetation, floodplains and water-bodies. On-going conversion has modified the thermal environment of the area, as indicated by increases in the magnitude and spatial distribution of LST over the study period. Our findings are based on Landsat imagery acquired at three temporal data points (1990, 2000, 2011). Our selection criteria required cloud-free imagery close to anniversary dates. Ideally, additional images should be employed to study the changes through time more finely [80] and closer to anniversary dates. However, we note that greater temporal resolution was severely impeded by an almost ubiquitous presence of cloud cover in the Landsat scenes visualised. Unfortunately, this is a problem in studies exploring urban thermal environments situated in tropical or sub-tropical regions of the world, a problem which has restricted numerous studies to small image sets in analysis of LST change across wide temporal and seasonal ranges [32,47,81,82].

6.1. Temporal comparison of LULC to LST

The highest mean LST in each study year were the built-up and bare-soil surfaces, which shared similar mean LST across study years likely due to similarity in albedo [25,83]. The mean LST of both surfaces continually increased over the study period, and the mean LST of natural surfaces such as water-bodies, floodplains and vegetation increased significantly when converted into these impervious surfaces. The higher mean temperature of these surfaces is likely due to the ability of impervious surfaces to retain solar heat [84]. Further, the removal of natural surfaces such as floodplains and vegetation to make way for these surfaces likely modified the surface energy balance and reduced evapotranspiration, resulting in an increase in the sensible heat flux and a reduction in latent heat flux [85] as well as modification to the heat storage and conductivity charactistics of the original surfaces [86].

Natural surfaces such as vegetation, cultivated land and floodplains exhibited moderate LST increases across the study period, possibly as a result of seasonal variation. Floodplains become highly inundated during certain periods of heavy rain [9], altering the thermal characteristics of the surface. The presence of prominent crop vegetation, extensive harvest activity between January and March [87], and moisture stress from pre-monsoonal drought [44,88] also results in fluctuations in land surface temperatures at different times of the year. The mean LST of water-bodies maintained a consistent temperature of approximately 19 °C across the study period, likely due to the consistently high thermal inertia of water surfaces [89]. Water-bodies only maintained consistent temperatures after seasonal variation was normalized across the study period. Without normalisation, water-body surface temperature increased and was significantly different across the study period, highlighting strong seasonal influence across our restricted, non-normalised Landsat image set.

A reduction of water-bodies and vegetated areas, which typically mitigate high surface temperatures due to differing albedos and heat storage capacity [1,90], are also likely to have contributed to an increase in the LST. Regardless, as a result of several decades of rapid urbanisation in Dhaka, impervious surfaces have expanded considerably. Considering that impervious materials such as concrete maintain a high thermal inertia and conductivity [25], high heat storage capacity [86] and can increase surface reflections and reduce wind dispersal in an urban area [91], the rapid development of these surfaces and the removal of natural surfaces has led to postively trending LSTs in Dhaka.

These findings reflect the results of similar studies in comparable subtropical or monsoonal climates. For instance, Xu et al. [92] investigated the influence of LULC change on LST of the subtropical Quanzhou region of south-eastern China over two decades using Landsat imagery. They found that LULC change had led to rapid urban expansion, causing natural surfaces to be converted into impervious surfaces, resulting in an urban heat island (UHI) effect. It was found through multivariate statistics that built-up surfaces contributed greatly to LST increase. Likewise, Weng [93], explored the influence of LULC change on LST in the subtropical Zhujiang Delta, China over a decade. Weng [93] found that land development raised surface radiant temperature by approximately 10^{o}C and found that this change indirectly reduced the biomass of the Zhujiang Delta. LST increases were highly correlated to urban expansion, particularly to the development of major roads. Importantly, simulated forecasts in Dhaka to 2029 indicate continued and rapid increases in LST [76] and reinforce both the negative influence of unmanaged urban growth on LST and the importance of maintaining natural surfaces.

Our results are strongly dependent on the accuracy of the land cover derivatives used over the three time periods, which were noted as having overall accuracies between 88 and 95%. Hence, we assume that, like Dewan and Corner [94], green space has been rapidly converted to predominantly impervious surfaces over the entire study period. However, this is in contrast to Raja [77] and Raja and Neema [95], who explored LULC change and LST in Dhaka across the period 1989–2010 and determined that vegetated and other natural surfaces actually increased in area over time (i.e., in 2010).

Almost equally consistent across these studies, are noted issues pertaining to seasonal influence on LST. Raja [77] and Raja and Neema [95] indicate unexpected area increases in some LULC types and decline in mean LST within their most recent study year (2010) may potentially be related to seasonal variations. Similarly, Dewan and Corner [94] attributed season to inflated mean LST of built-up surfaces in some years. Here we have applied and statistically validated the correction proposed by Zhou and Wang [24] for seasonal differences, avoiding these possible influences thus enabling more confident acquisition of non-anniversary date, cloud-free imagery in Dhaka. We encourage similar validation be carried out in other study areas.

Similarly, Ahmed et al. [76] indicated that reliance on a limited set of index-based parameters potentially reduced LST model strength when predicting LST dynamics in Dhaka and suggested improvements could be made using improved, or more, biophysical parameters. Based on our findings, use of LSMA-derived parameters offer stronger correlations with LST than traditional index-based parameters, and may therefore improve model strength. Furthermore, the continued advancement in modern satellites spectral resolution (e.g., Landsat 8, Sentinel 2), coupled with LSMA, could be applied to extract far more surface materials from imagery than index-based techniques, improving LULC maps and correlations with LST [96].

6.2. Comparison of LST and biophysical parameters

Univariate statistics indicated that the use of LSMA-derived biophysical parameters (GVF and ISA) were more highly correlated to LST than their index-based equivalents (NDVI and NDBI). This is particularly evident when comparing NDVI to GVF, and differences were most pronounced in 1990. NDBI was a stronger predictor of LST than NDVI, which has previously been reported [12] and is due to the comparatively low seasonal influence on impervious surfaces [97,98]. Similarly, ISA was a stronger predictor than GVF.

Despite the improvements that the LSMA method can provide for deriving accurate biophysical parameters and LST modelling, it is important to note that the user should make some considerations prior to use. First, the LSMA approach is a highly iterative and particularly elaborate process. This makes it prone to more human error when compared to the index-based approach. The requirement of expert knowledge is also a key factor in deriving accurate fraction images, limiting the use of this process to specialists. Furthermore, deriving urban impervious surface fraction imagery is highly prone to the 'mixed pixel problem' due to high pixel variability associated with built-up surfaces [99]. This makes the selection of accurate endmembers both difficult and time consuming during the process. To this end, it is reasonable to suggest that studies utilising LSMA to derive biophysical parameters should also derive NDVI or NDBI and compare to the results of LSMA to assess accuracy.

7. Conclusion

The increase in unmanaged urbanisation in Dhaka and its immediate surroundings has led to a continuous increase in LST as vegetation and floodplains are converted into either bare-soil or built-up surfaces. Two index-based biophysical parameters (NDVI and NDBI) were compared with two LSMA-based parameters or fraction surfaces (GVF and ISA). NDBI indicated a strong relationship with LST due to its heat retaining capacities. However, the LSMA parameters yielded stronger relationships with LST than the corresponding index-based parameters, particularly for vegetation (GVR>NDVI).

Acknowledgements

We are extremely grateful for the comments of two anonymous reviewers, which significantly helped to improve this paper.

Conflict of interest

All authors declare no conflicts of interest in this paper.

References

1. Grimm NB, Faeth SH, Golubiewski NE, et al. (2008) Global change and the ecology of cities. *Science* 319: 756-760.
2. United Nations (UN), World urbanization prospects: the 2011 revision. United Nations, 2012. Available from: http://www.un.org/en/desa/population/publications/pdf/urbanization/WUP2011_Report.pdf
3. United Nations Population Fund (UNFPA), The state of world population: 2011. United Nations Population Fund, 2011. Available from: http://www.unfpa.org/sites/default/files/pub-pdf/EN-SWOP2011-FINAL.pdf.
4. Black D, Henderson V (1999) A theory of urban growth. *JPE* 107: 252-284.
5. Dewan AM, Yamaguchi Y (2009) Land use and land cover change in Greater Dhaka, Bangladesh: Using remote sensing to promote sustainable urbanization. *Appl Geogr* 29: 390-401.

6. Rana MMP (2011) Urbanization and sustainability: challenges and strategies for sustainable urban development in Bangladesh. *Environment, Development and Sustainability* 13: 237-256.
7. Hasan S, Mulamoottil G (1994) Environmental problems of Dhaka City: a study of mismanagement. *Cities* 11: 195-200.
8. Azad A, Kitada T (1998) Characteristics of the air pollution in the city of Dhaka, Bangladesh in winter. *Atmospheric Environment* 32: 1991-2005.
9. Dewan AM, Corner RJ (2013) Introduction to Dhaka Megacity, In: Dewan A. M & Corner R. J, *Dhaka megacity: geospatial perspectives on urbanisation, environment and health*, 2 Eds., New York: Springer Science & Business Media, 1-48.
10. Foley JA, Defries R, Asner GP, et al. (2005) Global consequences of land use. *Science* 309: 570-574.
11. Voogt JA, Oke TR (1998) Effects of urban surface geometry on remotely-sensed surface temperature. *Int J Remote Sens* 19: 895-920.
12. Yuan F, Bauer ME (2007) Comparison of impervious surface area and normalized difference vegetation index as indicators of surface urban heat island effects in Landsat imagery. *Remote Sens Environ* 106: 375-386.
13. Kovats S, Akhtar H (2008) Climate, climate change and human health in Asian cities. *Environ Urban* 20: 165-175.
14. Patz JA, Olson SH (2006) Climate change and health: global to local influences on disease risk. *Ann Trop Med Parasit* 100: 535-549.
15. Shahid S (2009) Probable impacts of climate change on public health in Bangladesh. *Asia Pac J Public Health* 124: 432-444.
16. Hashizume M, Dewan AM, Sunahara T, et al. (2012) Hydroclimatological variability and dengue transmission in Dhaka, Bangladesh: a time-series study. *BMC Infect Dis* 12: 98.
17. Dewan AM, Corner R, Hashizume M, et al. (2014) Typhoid fever and its association with environmental factors in the Dhaka metropolitan area of Bangladesh: a spatial and time-series approach. *PLoS Negl Trop Dis* 7: 1998.
18. Byomkesh T, Nakagoshi N, Dewan AM (2011) Urbanization and green space dynamics in greater Dhaka, Bangladesh. *Landsc Ecol Eng* 8: 45-58.
19. Fortuniak K, Kłysik K, Wibig J (2005) Urban–rural contrasts of meteorological parameters in Łódź. *Theor Appl Climatol* 84: 91-101.
20. Wong NH, Yu C (2005) Study of green areas and urban heat island in a tropical city. *Habitat Int* 29: 547-558.
21. Saaroni H, Ben-Dor E, Bitan A, et al. (2000) Spatial distribution and microscale characteristics of the urban heat island in Tel-Aviv, Israel. *Landscape Urban Plan* 48: 1-18.
22. Yow DM (2007) Urban heat islands: observations, impacts and adaptation. *Geography Compass* 1: 1227-1251.
23. Weng Q (2009) Thermal infrared remote sensing for urban climate and environmental studies: methods, applications and trends. *ISPRS J Photogramm* 64: 335-344.
24. Zhou X, Wang YC (2011) Dynamics of land surface temperature in response to land-use/cover change. *Geogr Res* 49: 23-36.
25. Carnahan WH, Larson RC (1990) An analysis of an urban heat sink. *Remote Sens Environ* 33: 65-71.

26. Streutker DR (2002) A remote sensing study of the urban heat island of Houston, Texas. *Int J Remote Sens* 23: 2595-2608.
27. Walawender JP, Szymanowski M, Hajto MJ, et al. (2013) Land surface temperature patterns in the urban agglomeration of Krakow (Poland) derived from landsat-7/etm+ data. *Pure Appl Geophys* 4: 23-54.
28. Voogt JA, Oke TR (2003) Thermal remote sensing of urban climates. *Remote Sens Environ* 86: 370-384.
29. Carlson TN, Gillies RR, Perry EM (1994) A method to make use of thermal infrared temperature and NDVI measurements to infer surface soil water content and fractional vegetation cover. *Remote Sens Rev* 9: 161-173.
30. Zha Y, Gao J, Ni S (2003) Use of normalized difference built-up index in automatically mapping urban areas from TM imagery. *Int J Remote Sens* 24: 583-594.
31. Weng Q (2008) Medium spatial resolution satellite imagery for estimating and mapping urban impervious surfaces using LSMA and ANN. *IEEE T Geosci Remote* 46: 2397-2406.
32. Ma Y, Kuang Y, Huang N (2010) Coupling urbanization analyses for studying urban thermal environment and its interplay with biophysical parameters based on TM/ETM+ imagery. *Int J Appl Earth Obs* 12: 110-118.
33. Adams J (1995) Classification of multispectral images based on fractions of endmembers: application to land-cover change in the Brazilian Amazon. *Remote Sens Environ* 52: 137-154.
34. Brown M, Lewis HG, Gunn SR (2000) Linear spectral mixture models and support vector machines for remote sensing. *IEEE T Geosci Remote* 38: 2346-2360.
35. Rashid H (1978) Geography of Dhaka, In: Rashid, H, *Geography of Bangladesh*, 2 Eds., Dhaka: University Press, 78-94.
36. Tareq SM, Maruo M, Ohta K (2013) Characteristics and role of groundwater dissolved organic matter on arsenic mobilization and poisoning in Bangladesh. *Phys Chem Earth* 1: 77-84.
37. Water Resources Planning Organization (WARPO), Datum and map projections for GIS and GPS applications in Bangladesh. Water Resources Planning Organization, 1996. Available from: http://www.cegisbd.com/pdf/tn10DatumMapProjections.pdf.
38. Chander G, Markham B (2003) Revised landsat-5 TM radiometric calibration procedures and postcalibration dynamic ranges. *IEEE T Geosci Remote* 41: 2674-2677.
39. Chander G, Markham BL, Helder DL (2009) Summary of current radiometric calibration coefficients for Landsat MSS, TM, ETM+ and EO-1 ALI sensors. *Remote Sens Environ* 113: 893-903.
40. Chavez P (1996) Image-based atmospheric corrections: revisited and improved. *Photogramm eng rem s* 62: 1025-1035.
41. IDRISI Selva—GIS and Image Processing Software (Version 17), (2012). Worcester, Massachusetts: Clark Laboratories.
42. Anderson R, Hardy EE, Roach JT, et al. (1976) A land use and land cover classification system for use with remote sensor data, In: United States Geological Survey (USGS), *Professional Papers Vol. 964*, 1 Eds., Sioux Falls: USGS Professional Printing, 41-78.
43. Mas J (1999) Monitoring land-cover changes: a comparison of change detection techniques. *Int J Remote Sens* 20: 139-152.
44. Streatfield P, Karar Z (2008) Population challenges for Bangladesh in the coming decades. *JHPS* 26: 261-272.

45. Qin Z, Karnieli A, Berliner P (2001) A mono-window algorithm for retrieving land surface temperature from Landsat TM data and its application to the Israel-Egypt border region. *Int J Remote Sens* 22: 3719-3746.
46. Jiménez-Muñoz JC, Sobrino JA (2003) A generalised single channel method for retrieving land surface temperature from remote sensing data. *J Geophys Res* 108: 4688.
47. Chen XL, Zhao HM, Li P, et al. (2006) Remote sensing image-based analysis of the relationship between urban heat island and land use/cover changes. *Remote Sens Environ* 104: 133-146.
48. Lo CP, Quattrochi DA (2003) Land-use and land-cover change, urban heat island phenomenon, and health implications. *Photogramm Eng Rem S* 69: 1053-1063.
49. Tran H, Uchihama D, Ochi S, et al. (2006) Assessment with satellite data of the urban heat island effects in Asian mega cities. *Int J Appl Earth Obs* 8: 147-156.
50. Artis DA, Carnahan WH (1982) Survey of emissivity variability in thermography of urban areas. *Remote Sens Environ* 12: 313-329.
51. Sobrino JA, Jiménez-Muñoz JC, Sòria G, et al. (2008) Land surface emissivity retrieval from different VNIR and TIR sensors. *Int J Remote Sens* 46: 316-327.
52. Xiao R, Ouyang Z, Zheng H, et al. (2007) Spatial pattern of impervious surfaces and their impacts on land surface temperature in Beijing, China. *J Environ Sci* 19: 250-256.
53. Mackey CW, Lee X, Smith RB (2012) Remotely sensing the cooling effects of city scale efforts to reduce urban heat island. *Build Environ* 49: 348-358.
54. Nichol JE (1994) Approach to a GIS-Based monitoring survey of microclimate of Singapore's housing estates. *Cities* 60: 43-56.
55. Sobrino JA, Jiménez-Muñoz JC, Paolini L (2004) Land surface temperature retrieval from Landsat TM 5. *Remote Sens Environ* 90: 434-440.
56. Carlson TN, Ripley DA (1997) On the relation between NDVI, fractional vegetation cover and leaf area index. *Remote Sens Environ* 62: 241-252.
57. Sobrino JA, Caselles V, Becker F (1990) Significance of the remotely sensed thermal infrared measurements obtained over a citrus orchard. *ISPRS J Photogramm* 44: 343-354.
58. Walawender JP, Hajto MJ, Iwaniuk P (2012) A new ArcGIS toolset for automated mapping of land surface temperature with the use of landsat satellite data. *IEEE International Geoscience and Remote Sensing Symposium* 2012: 4371-4374.
59. Carlson TN, Arthur ST (2000) The impact of land use–land cover changes due to urbanization on surface microclimate and hydrology: a satellite perspective. *Global Planet Change* 25: 49-65.
60. Weng Q, Lu D, Schubring J (2004) Estimation of land surface temperature–vegetation abundance relationship for urban heat island studies. *Remote Sens Environ* 89: 467-483.
61. Zhang X, Zhong T, Wang K, et al. (2009) Scaling of impervious surface area and vegetation as indicators to urban land surface temperature using satellite data. *Int J Remote Sens* 30: 841-859.
62. Huete A, Didan K, Miura T, et al. (2002) Overview of the radiometric and biophysical performance of the MODIS vegetation indices. *Remote Sens Environ* 83: 195-213.
63. Sun F, Sun W, Chen J, et al. (2012). Comparison and improvement of methods for identifying waterbodies in remotely sensed imagery. *Int J Remote Sens* 33: 6854-6875.
64. ArcGIS—GIS Software (Version 10.1), (2012). Redlands, California: Environmental Systems Research Institute (ESRI).
65. Yang X, Liu Z (2005) Use of satellite-derived landscape imperviousness index to characterize urban spatial growth. *Computers, Environment and Urban Systems* 29: 524-540.

66. ENVI—GIS software (Version 4.8), (2012). Boulder, Colorado: Harris Geospatial Solutions.
67. Wu C (2004) Normalized spectral mixture analysis for monitoring urban composition using ETM+ imagery. *Remote Sens Environ* 93: 480-492.
68. Green AA, Berman M, Switzer P, et al. (1988) A transformation for ordering multispectral data in terms of image quality with implications for noise removal. *IEEE T Geosci Remote* 26: 65-74.
69. Boardman J (1993) Automating spectral unmixing of AVIRIS data using convex geometry concepts. *4th Annual JPL Airborne Geoscience Conference and Worskhop* 2: 2-5.
70. Boardman J, Kruse F, Green R (1995) Mapping target signatures via partial unmixing of AVIRIS data. *5th Annual JPL Airborne Geoscience Conference and Worskhop* 3: 3-6.
71. Tukey JW (1953) The problem of multiple comparisons. In: Unpublished Manuscript, Trenton: Princeton University, 1-38.
72. Liu H, Weng Q (2008) Seasonal variations in the relationship between landscape pattern and land surface temperature in Indianapolis, USA. *Environ Monit Assess* 144: 199-219.
73. National Aeronautics and Space Administration, Landsat 7 science data users handbook. National Aeronautics and Space Administration, 2000. Available from: https://landsat.gsfc.nasa.gov/wp-content/uploads/2016/08/Landsat7_Handbook.pdf.
74. SPSS- Statistics Software (Version 22), (2012). Armonk, New York: IBM Corporation.
75. Cohen J, Cohen P, West S, et al. (2013) Data-Analytic Strategies Using Multiple Regression/Correlation, In: Cohen J, Cohen P, Applied multiple regression/correlation analysis for the behavioural sciences, 3 Eds., London: Lawrence Erlbaum Associates, 151-192.
76. Ahmed B, Kamruzzaman M, Zhu X, et al. (2013) Simulating land cover changes and their impacts on land surface temperature in Dhaka, Bangladesh. *Remote Sens* 5: 5969-5998.
77. Raja DR (2012) Spatial analysis of land surface temperature in Dhaka metropolitan area. *J Bangladesh Institute of Planners* 5: 151-167.
78. Xiao H, Weng Q (2007) The impact of land use and land cover changes on land surface temperature in a karst area of China. *J Environ Manage* 85: 245-257.
79. Xu H, Dongfeng L, Tang F (2013) The impact of impervious surface development on land surface temperature in a subtropical city: Xiamen, China. *Int J Climatol* 33: 1873-1883.
80. Li Y, Zhang H, Kainz W (2012) Monitoring patterns of urban heat islands of the fast-growing Shanghai metropolis, China: Using time-series of Landsat TM/ETM+ data. *Int J Appl Earth Obs* 19: 127-138.
81. Tan KC, San-Lim H, Matjafri MZ, et al. (2010) Landsat data to evaluate urban expansion and determine land use/land cover changes in Penang Island, Malaysia. *Environ Earth Sci* 60: 1509-1521.
82. Li J, Wang J, Ma J, et al. (2009) Remote sensing evaluation of urban heat island and its spatial pattern of the Shanghai metropolitan area, China. *Ecol Complex* 6: 413-420.
83. Li J, Song C, Cao L, et al. (2011) Impacts of landscape structure on surface urban heat islands: a case study of Shanghai, China. *Remote Sens Environ* 115: 3249-3263.
84. Roth M, Oke TR, Emery WJ (1989) Satellite-derived urban heat islands from three coastal cities and the utilization of such data in urban climatology. *Int J Remote Sens* 10: 1699-1720.
85. Owen TW, Carlson TN, Gillies RR (1998) An assessment of satellite remotely-sensed land cover parameters in quantitatively describing the climatic effect of urbanization. *Int J Remote Sens* 19: 1663-1681.

86. Cao L, Li P, Zhang L, et al. (2002) Remote sensing image-based analysis of the relationship between urban heat island and vegetation fraction. *The International Archives of the Photogrammetry, Remote Sensing and Spatial Information Sciences* 1: 1379-1383.
87. Giri C, Pengra B, Zhu Z, et al. (2007) Monitoring mangrove forest dynamics of the sundarbans in Bangladesh and India using multi-temporal satellite data from 1973 to 2000. *Estuar Coast Shelf S* 73: 91-100.
88. Bangladesh Department of Environment Climate Change Cell (2006) *Bangladesh climate change impacts and vulnerability: a synthesis*. Dhaka, Department of Environment Publishing.
89. Goward SN (1981) Thermal behavior of urban landscapes and the urban heat island. *Phys Geogr* 2: 19-33.
90. Grimmond CSB (2005) Progress in measuring and observing the urban atmosphere. *Theor Appl Climatol* 84: 3-22.
91. Oke TR (1982) The energetic basis of the urban heat island. *J Roy Meteor Soc* 108: 1-24.
92. Xu H, Ding F, Wen X (2009) Urban expansion and heat island dynamics in the Quanzhou region, China. *IEEE J-STAEORS* 2: 74-79.
93. Weng Q (2001) A remote sensing GIS evaluation of urban expansion and its impact on surface temperature in the Zhujiang Delta, China. *Int J Remote Sens* 22: 1999-2014.
94. Dewan A, Corner R (2014). Impact of land use and land cover changes on urban land surface temperature, In: Dewan AM, Corner RJ, *Dhaka megacity: geospatial perspectives on urbanisation, environment and health*, 2 Eds., New York: Springer Science & Business Media, 219-238.
95. Raja DR, Neema MN (2013) Impact of urban development and vegetation on land surface temperature of Dhaka city. *Comp Sci Appl* 7973: 351-367.
96. Weng Q, Hu X, Lu D (2008). Extracting impervious surfaces from medium spatial resolution multispectral and hyperspectral imagery: a comparison. *Int J Remote Sens* 29: 3209-3232.
97. Song C, Woodcock CE, Seto KC (2001) Classification and change detection using landsat TM data. *Remote Sens Environ* 75: 230-244.
98. Weng Q, Lu D (2008) Extracting impervious surfaces from medium spatial resolution multispectral and hyperspectral imagery: a comparison. *Int J Remote Sens* 29: 3209-3232.
99. Xu H (2008) A new remote sensing index for fastly extracting impervious surface information. *GIS* 8: 12-28.

AIMS Press